Dalton
www.rsc.org/dalton

Electrocatalysis of hydrogen production by active site analogues of the iron hydrogenase enzyme: structure/function relationships †

Daesung Chong, Irene P. Georgakaki, Rosario Mejia-Rodriguez, Jean Sanabria-Chinchilla, Manuel P. Soriaga and Marcetta Y. Darensbourg *

Texas A&M University, Department of Chemistry, College Station, Texas 77843, USA. E-mail: marcetta@mail.chem.tamu.edu; Fax: 979-845-0158; Tel: 979-845-5417

Received 17th April 2003, Accepted 30th May 2003
First published as an Advance Article on the web 22nd September 2003

A series of binuclear $Fe^{I}Fe^{I}$ complexes, $(\mu\text{-SEt})_2[Fe(CO)_2L]_2$ (L = CO (**1**), PMe_3 (**1-P**)), $(\mu\text{-SRS})[Fe(CO)_2L]_2$ (R = CH_2CH_2 (μ-edt): L = CO (**2**), PMe_3 (**2-P**); R = $CH_2CH_2CH_2$(μ-pdt): L = CO (**3**), PMe_3 (**3-P**); and R = *o*-$CH_2C_6H_4CH_2$ (μ-*o*-xyldt): L = CO (**4**), PMe_3 (**4-P**)), that serve as structural models for the active site of Fe-hydrogenase are shown to be electrocatalysts for H_2 production in the presence of acetic acid in acetonitrile. The redox levels for H_2 production were established by spectroelectrochemistry to be $Fe^{0}Fe^{0}$ for the all-CO complexes and $Fe^{I}Fe^{0}$ for the PMe_3-substituted derivatives. As electrocatalysts, the PMe_3 derivatives are more stable and more sensitive to acid concentration than the all-CO complexes. The electrocatalysis is initiated by electrochemical reduction of these diiron complexes, which subsequently, under weak acid conditions, undergo protonation of the reduced iron center to produce H_2. An $(\eta^2\text{-}H_2)Fe^{II}\text{–}Fe^{0/I}$ intermediate is suggested and probable electrochemical mechanisms are discussed.

Introduction

Hydrogenase enzymes control dihydrogen metabolism in a wide variety of rudimentary microorganisms.[1] These complex biomolecules have long intrigued chemists and engineers for the possibility that they might hold the key to a viable macroscale hydrogen economy.[2,3] Hydrogenases have evolved to perform both H_2 production and H_2 uptake reversibly in the simplest of reactions, $2\ H^+ + 2\ e^- \rightleftharpoons H_2$, which in the natural systems occur at neutral pH and in a redox range of −100 to −550 mV.[1,2] The H_2-production process is of obvious importance to the ready accessibility of H_2 and is most typically carried out by iron-only hydrogenase, [Fe]H_2ase; the good H_2-uptake by nickel–iron hydrogenase, [NiFe]H_2ase, has implications for fuel cell development.[4,5] The confluence of recent progress in the fundamental sciences of molecular biology, genetics, and protein crystallography with the need for alternatives to fossil fuels provides renewed stimulus for research in this area.[2]

The iron-only hydrogenase, [Fe]H_2ase, is remarkable in its efficiency for H_2 production[6] as well as in the formulation/construction of its active site.[7–9] As in the [NiFe]H_2ase,[10] [Fe]H_2ase is outfitted with a series of iron–sulfur clusters that "wire" the active site to the electron donor/acceptor protein docked into the periphery of the redox-active enzyme. For [Fe]H_2ase, X-ray crystallography, with support from vibrational spectroscopy, has established the presence of diatomic ligands, CO and CN^-, in a binuclear active site which is shown in Fig. 1.[7–9] Compositional/structural models which serve as spectroscopic reference points for the active site can be readily accessed from $(\mu\text{-}S_2)Fe_2(CO)_6$.[11] Derivatives in the form of $(\mu\text{-E})(\mu\text{-pdt})[Fe^{II}(CO)_2PMe_3]_2^+$ (E = H, SMe; pdt = $SCH_2CH_2CH_2S$) have demonstrated ability to promote the same isotopic scrambling reaction[12–14] as used in activity assays for the enzyme, eqn. (1).

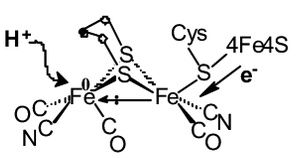

Fig. 1 Representation of [Fe]hydrogenase active site in the reduced form and its role in H^+/e^- uptake.

$$H_2 + D_2O \rightleftharpoons HD + HOD \qquad (1)$$

Key to this functional biomimicry is the requirement of light which generates an open site necessary for $\eta^2\text{-}H_2$ binding to d^6 Fe^{II} complexes.[15] Thus the binuclear $(\eta^2\text{-}H_2)Fe^{II}Fe^{II}$ intermediate in these H_2ase-like activity studies mimics the $(\eta^2\text{-}H_2)Fe^{II}$ interaction of the distal iron of the oxidized form of the enzyme proposed to be in a mixed-valent $Fe^{II}Fe^{I}$ redox level.[16–18]

As illustrated in Fig. 1, the enzyme active site in the reduced form has an available coordination position on the distal iron[8] (the iron in the dinuclear complex furthest removed from the iron–sulfur cluster that shuttles electrons into or out of the active site) that may be occupied by H_2 or H^-, dependent on the direction of reactivity. The spectroscopically-supported oxidation state assignment of this diamagnetic, reduced form of the enzyme is $Fe^{I}Fe^{I}$.[16,18] However, the asymmetric Fe–Fe bond electron density distribution makes the distal iron even lower valent, depicted in Fig. 1 in the extreme oxidation state of Fe^0. This apparent open site in the reduced form of the enzyme is occupied by a labile H_2O molecule in the oxidized, mixed-valent $Fe^{II}Fe^{I}$ redox level[16–18] that is responsible for H_2 binding and activation.

Thus the production of H_2 is presumed to occur *via* protonation of an $Fe^{II}\text{–}H^-$, itself deriving from a precursor Fe^0 species *via* protonation, eqn. (2).

$$[Fe^0\text{–}Fe^{I}] + H^+ \longrightarrow [H\text{–}Fe^{II}\text{–}Fe^{I}] + H^+ \longrightarrow [(\eta^2\text{-}H_2)Fe^{II}\text{–}Fe^{I}] \qquad (2)$$

In order to provide precedent for such proposed H_2-production activity, a series of $(\mu\text{-SRS})[Fe^{I}(CO)_2L]_2$ complexes were used to explore the potential of these structural models for H_2 production. A detailed electrochemical study of the $Fe^{I}Fe^{I}$ dithiolate models and the electrocatalytic H_2 production at the $Fe^{0}Fe^{I}$ and $Fe^{0}Fe^{0}$ redox level in the presence of a weak acid is discussed in this paper.

† Based on the presentation given at Dalton Discussion No. 6, 9–11th September 2003, University of York, UK.

Electronic supplementary information (ESI) available: Cyclic voltammograms for **1** to the anodic direction, and for **4-P** with acetic acid. *In situ* IR spectra during bulk electrolysis for **2** with acetic acid and reduction and re-oxidation process for **1** in the absence of acid. See http://www.rsc.org/suppdata/dt/b3/b304283a/

DOI: 10.1039/b304283a

Experimental

Materials

Starting materials, (μ-SEt)$_2$[Fe(CO)$_2$L]$_2$ (L = CO (**1**), PMe$_3$ (**1-P**)), (μ-edt)[Fe(CO)$_2$L]$_2$ (L = CO (**2**), PMe$_3$ (**2-P**)), (μ-pdt)-[Fe(CO)$_2$L]$_2$ (L = CO (**3**), PMe$_3$ (**3-P**)) and (μ-*o*-xyldt)-[Fe(CO)$_2$L]$_2$ (L = CO (**4**), PMe$_3$ (**4-P**)) were prepared by the literature methods.[13,19,20] Acetonitrile was distilled once from CaH_2 and once from P_2O_5, and then freshly distilled from CaH_2 immediately before use. The all-CO complexes were air-stable while the PMe$_3$ derivatives were stored, weighed and transferred in an Ar-filled glove box.

Electrochemistry

Electrochemical measurements were made using a BAS 100A potentiostat. All voltammograms were obtained in a conventional and a gas-tight three-electrode cell under Ar, N_2, or CO atmosphere. The working electrode was a glassy carbon disk (0.071 cm^{-1}) polished with 1 μm diamond paste and sonicated in H_2O for 15 min. All potentials were measured in 0.1 M *n*-Bu_4NBF_4 solution in CH_3CN and they are reported relative to the normal hydrogen electrode (NHE). Bulk electrolyses for electrocatalytic reaction were done using an EG&G Model 273 potentiostat and Galvanostat. Electrocatalytic experiments were carried out under argon or nitrogen atmosphere for 1 h on a vitreous carbon rod (A = 3.34 cm^2) in a gas-tight H-type electrolysis cell containing *ca.* 10 mL CH_3CN which was 2.5 mM in the diiron complexes and 0.1 M in *n*-Bu_4NBF_4.

Spectroscopy

Infrared spectroscopic monitoring experiments during the course of bulk electrolysis were performed by use of a ReactIR™ 1000 equipped with an MCT detector and 30 bounce SiCOMP *in situ* probe and purchased from Applied Systems Inc. The *in situ* IR probe was immersed in a self-designed, 50 mL, electrolysis cell as shown in Fig. 2-(I). The EPR spectrum was recorded on a Bruker X-band EPR spectrometer (model ESP 300E) with Oxford Liquid Helium/Nitrogen cryostat at 10 K, 1 mW power and 0.1 mT modulated amplitude.

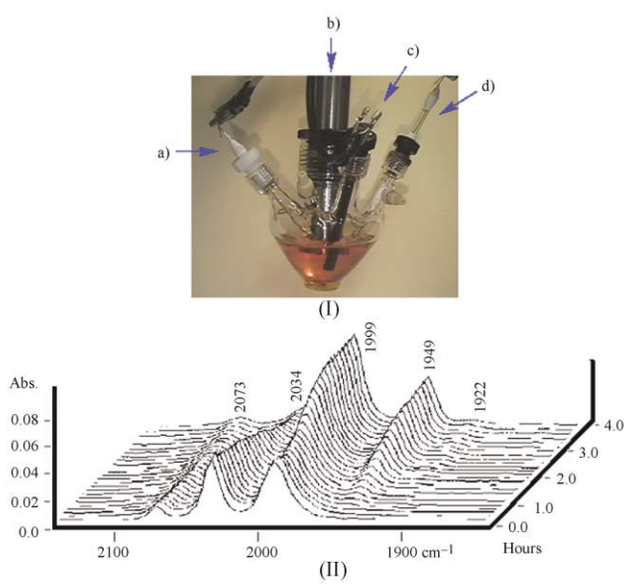

Fig. 2 (I) The *in situ* IR/electrochemical cell: (a) reference electrode (Ag/Ag$^+$), (b) *in situ* IR probe (ReactIR™), (c) working electrode (carbon rod) and (d) counter electrode (Pt); and (II) sample stacked plot IR spectra for the reduction process at −1.34 V of complex **1** (7.5 mM).

Results and discussion

Electrochemistry/cyclic voltammograms

The series of diiron dithiolates used in this study is given in Table 1 along with infrared data in the CO stretching region. All complexes in the series have been structurally characterized by single crystal X-ray crystallography,[12,13,21] and representatives of those structures are displayed as stick drawings in Fig. 3. A combination of steric and electronic effects accounts for the specific geometries observed in the PMe$_3$ substituted derivatives.[13] While the three-band ν(CO) pattern in the IR is similar for each of the all-CO species, differences arise for the phosphine-substituted series which depend on the positions of the PMe$_3$ ligands.[13] Reflecting the electron-donating ability of the phosphines (which is similar to cyanides), the average ν(CO) value is *ca.* 100 cm^{-1} lower in the PMe$_3$-substituted complexes as compared to the all-CO complexes. The ν(CO) infrared spectral values within the all-CO and the PMe$_3$-substituted subsets show no significant differences for the μ-SRS derivatives, however the μ-SEt complexes appear to have slightly lower ν(CO) values in each subset, Table 1.

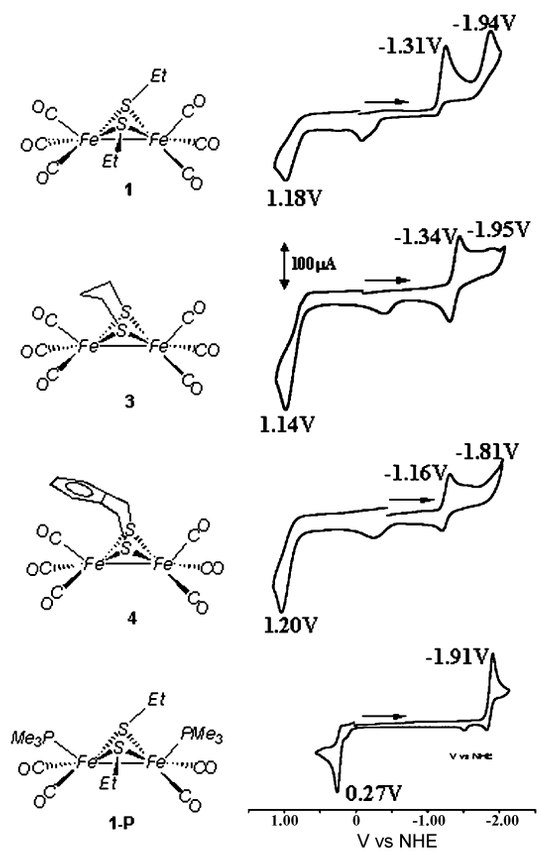

Fig. 3 Cyclic voltammograms of a series of complexes **1**, **3**, **4** and **1-P** in CO-saturated CH_3CN solution (0.1 M *n*-Bu_4NBF_4) with electrochemical parameters as described in Table 1.

The cyclic voltammograms shown in Fig. 3 were recorded in CO-saturated CH_3CN solution which gave better defined waves; they were initiated from the rest potentials and proceed as indicated in the cathodic direction. The all-CO species display two reduction events that are typical of all members of the series. A quasi-reversible or electrochemically irreversible reduction (E_1) is observed for the all-CO species in the range of −1.16 to −1.34 V, in agreement with the values obtained by Pickett and co-workers,[22] and an irreversible event (E_2) is in the range of −1.81 to −1.95 V. The assignment of the first event to a one-electron reduction process $Fe^{I}Fe^{I} + e^- \longrightarrow Fe^{I}Fe^{0}$ is supported by bulk electrolysis and IR data described below. The second reduction event is proposed to correspond to the

Table 1 Listing of ν(CO) infrared and electrochemical parameters[a] for (μ-SRS)[Fe(CO)$_2$L]$_2$ and (μ-SR)$_2$[Fe(CO)$_2$L]$_2$ complexes in CH$_3$CN

L = CO	ν(CO)/cm^{-1}	E_{pc} *vs.* NHE/V E_1: $Fe^IFe^I \longrightarrow Fe^0Fe^I$ (E_2: $Fe^0Fe^I \longrightarrow Fe^0Fe^0$)	E_{pa} *vs.* NHE/V $Fe^IFe^I \longrightarrow Fe^{II}Fe^I$
(μ-SEt)$_2$, **1**	2073 (m), 2034 (vs), 1992 (s)	−1.31 (−1.94)	1.18
(μ-edt), **2**	2087 (m), 2038 (vs), 1997 (s)	−1.30 (−1.84)	1.29
(μ-pdt), **3**	2074 (m), 2036 (vs), 1995 (s)	−1.34 (−1.95)	1.14
(μ-*o*-xyldt), **4**	2076 (m), 2040 (vs), 1999 (s)	−1.16 (−1.81)	1.20
L = PMe$_3$			
(μ-SEt)$_2$, **1-P**	1977 (s), 1931 (m), 1908 (s)	−1.91	0.27
(μ-edt), **2-P**	1982 (s), 1944 (s), 1908 (s), 1896 (m,br)	−1.87	0.34
(μ-pdt), **3-P**	1979 (m), 1942 (s), 1898 (s)	−1.85	0.34
(μ-*o*-xyldt), **4-P**	1983 (m), 1948 (s), 1903 (s)	−1.80	0.35

[a] CH$_3$CN solution (0.1 M *n*-Bu$_4$NBF$_4$) with a glassy carbon working electrode (A = 0.071 cm^2) to NHE using Cp$_2$Fe/Cp$_2$Fe$^+$ standard ($E_{1/2}$ = 0.40 V). Counter electrode: Pt. Scan rate: 0.2 V s^{-1}. SRS: μ-edt = SCH$_2$CH$_2$S, μ-pdt = SCH$_2$CH$_2$CH$_2$S, μ-*o*-xyldt = SCH$_2$–C$_6$H$_4$–CH$_2$S.

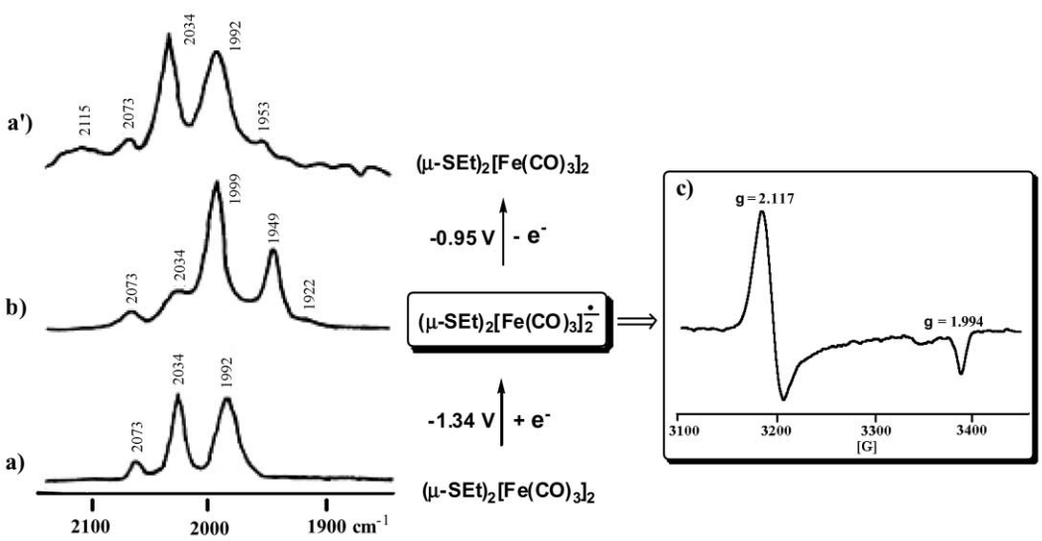

Fig. 4 *In situ* IR spectra during bulk electrolysis for **1** (7.5 mM). (a) neutral starting complex, (b) following reduction (E_{app} = −1.34 V), (a′) re-oxidation (E_{app} = −0.95 V) in 0.1 M *n*-Bu$_4$NBF$_4$ solution in CH$_3$CN and (c) EPR spectrum of a sample from (b).

Fe^IFe^0 + e$^-$ ⟶ Fe^0Fe^0 process. The PMe$_3$-derivatives **1-P** through **4-P** show one reduction event at *ca.* −1.9 V that is assigned to the one-electron reduction of Fe^IFe^I to Fe^IFe^0. Its appearance at more negative potentials than that corresponding to the all-CO complexes is consistent with the better donor character of the PMe$_3$ ligand relative to CO. At room temperature, controlled-potential coulometry of all complexes at each cathodic peak potential in the absence of added acid shows net consumption of about 0.95 electron per molecule.

The first reduction for complexes **3** and **4** show greater reversibility than complex **1**. The second reduction, E_2, is however better defined in **1**. The peak current of these redox couples is proportional to the square root of the scan rate (50–1000 mV s^{-1}), which indicates that the electrochemical processes are diffusion-controlled.[23]

Notable in the cyclic voltammograms for compounds **1**, **3** and **4** in Fig. 3 is a small irreversible event at *ca.* 0.0 V which appears only after cycling through the nearest reduction wave. It is assumed to result from a reduction-derived decomposition product (see ESI †). As the electrochemistry is performed under CO, the mononuclear [(EtS)Fe(CO)$_4$]$^-$ which has an irreversible oxidation wave about 0.07 V is a likely decomposition product.[24]

Also observed for each member of the series is an irreversible anodic or oxidative event which is displaced positively by *ca.* 2.2–2.6 V from the E_1 cathodic feature for all species, Fig. 3. As expected, the PMe$_3$ derivatives destabilize the Fe^IFe^0 form and stabilize the Fe^IFe^{II} as compared to the all-CO parent species. Minor differences in positions of either the cathodic or anodic events within the series are not readily correlated with the μ-SRS or μ-SR bridges; as mentioned above, the ν(CO) infrared spectral values are similar within a subset.

Spectroelectrochemistry

The E_1 process Fe^IFe^I ⟶ Fe^IFe^0 for complexes **1**, **3** and **4** is supported by spectroelectrochemical monitors using a ReactIR™ for *in situ* infrared monitoring of solutions during the course of bulk electrolysis (Figs. 2-II, 4 and ESI †). For example, electrolysis of a CO-saturated[25] CH$_3$CN solution of **1** at an applied potential of −1.34 V over the course of 4 h resulted in a loss of intensity of the three ν(CO) IR bands of the neutral complex (2073, 2034 and 1992 cm^{-1}, Fig. 4(a)) with growth of bands at 1999, 1949 and 1922 cm^{-1}, Fig. 4(b). On anodic electrolysis at −0.95 V the original IR spectrum was regenerated along with a minor amount of a species with infrared bands at 2115 and 1953 cm^{-1} (Fig. 4(a′)). While the structure of the one-electron reduced species is not known, that it is an anion of similar structure to that of the neutral starting material is a reasonable conclusion based on the IR spectral changes. Furthermore, the EPR spectrum (Fig. 4(c)) of a sample withdrawn from this solution displays an axial EPR signal ($g_\perp$ = 2.117 and $g_{||}$ = 1.994) indicative of an odd-electron species (Fe^IFe^0), and consistent with the one-electron occupancy of the Fe–Fe antibonding LUMO.[22,26] On addition of acid to the reduced species the EPR signal disappears and the

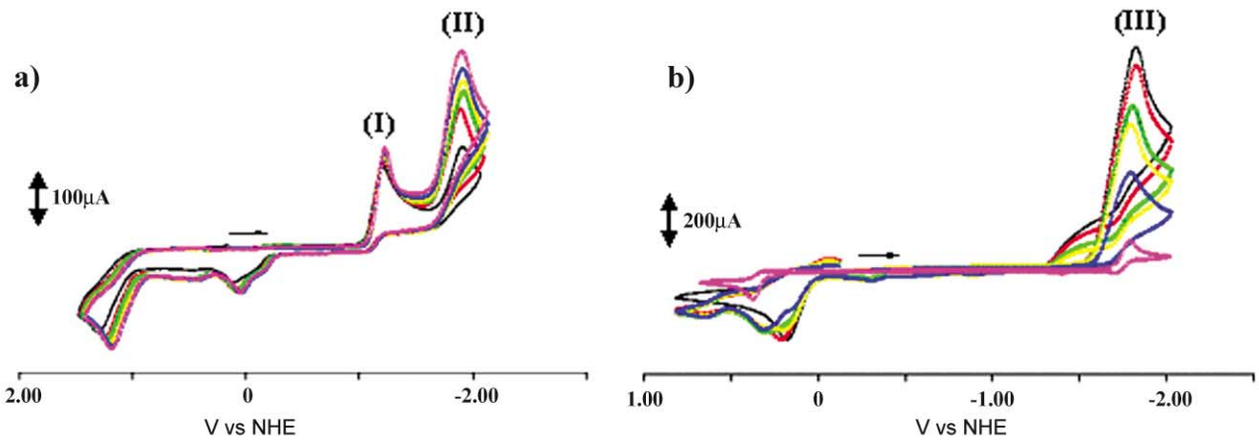

Fig. 5 Cyclic voltammograms of (a) complex **1** (2.5 mM) with HOAc (0–100 mM) and (b) **1-P** (2.5 mM) with HOAc (0–100 mM) in 0.1 M *n*-Bu_4NBF_4 in CH_3CN and with electrochemical parameters as described in Table 1. (I): Fe^IFe^I/Fe^0Fe^I, *ca.* −1.31 V; (II): Fe^0Fe^I/Fe^0Fe^0, *ca.* −1.94 V; (III): Fe^IFe^I/Fe^0Fe^I, *ca.* −1.91 V.

starting complex is reclaimed. The reversible chemical behavior is incongruent with the observed irreversible electrochemical response of complex **1** at the $Fe^IFe^I \longrightarrow Fe^IFe^0$ reduction event. At this time we have no explanation for this result.

Electrocatalysis of H_2 production

Controlled-potential electrolyses were performed in an H-type cell with a rod type glassy carbon electrode (A = 3.34 cm^2). Under the same conditions, acetic acid in CH_3CN (pK_a = 22.6)[27] is reduced at a potential of −2.2 V. For the all-CO complexes, **1**–**4**, the current height of the first redox wave (E_1 = −1.2 ± 0.1 V, Fig. 5(a)-(I)) shows a slight increase with added increments of acid while the second redox wave (E_2 = −1.9 ± 0.05 V, Fig. 5(a)-(II)) shows a significant electrocatalytic response. The current height of the single cathodic event at *ca.* −1.85 ± 0.05 V of the PMe_3-derivatives increases linearly with the concentration of acetic acid, Fig. 5(b) and 6. The steeper slope displayed by the PMe_3-derivative, **1-P**, Fig. 6, is indicative of its greater sensitivity to acid concentration compared to the all-CO complex **1**. This is consistent with a more stable reaction intermediate of the PMe_3 complex, presumably $H–Fe^{II}$. The electrolysis of complexes **1**, **1-P** and **4-P** at −1.96 V, −1.93 V and −1.85 V, respectively, in the presence of acetic acid (100 mM) for 1 h consumes 12 (*ca.* 6 turnovers h^{-1}), 34 (*ca.* 17 turnovers h^{-1}) and 60 (*ca.*30 turnovers h^{-1}) electrons per molecule, respectively. These observations are typical of electrocatalytic reactions.[23,28–33]

The gas which evolved during electrolysis was directed into an NMR tube, purging the CD_2Cl_2 solvent for 20 min. The ^1H NMR spectrum of this sample showed one resonance at 4.61 ppm for dissolved H_2.[12–14] A reasonable conclusion is that electrochemical reduction of the diiron complexes initiates the electrocatalysis, followed by protonation of the reduced iron center to produce H_2.

In the absence of acid, the cyclic voltammograms of the Fe^I-Fe^I complexes **1**–**4** and **1-P**–**4-P** measured in CO-saturated or N_2-saturated CH_3CN solution are fairly similar. In the presence of acid under N_2 an electrochemical response at −1.45 V appeared. The new event was not present in CO-saturated CH_3CN (Fig. 7). This observation is interpreted to signify that the oxidative addition of a proton to the reduced Fe^0Fe^I, to form $H–Fe^{II}–Fe^I$, prompts CO mobility and replacement by CH_3CN[34] giving rise to an additional and more negative electrochemical response.

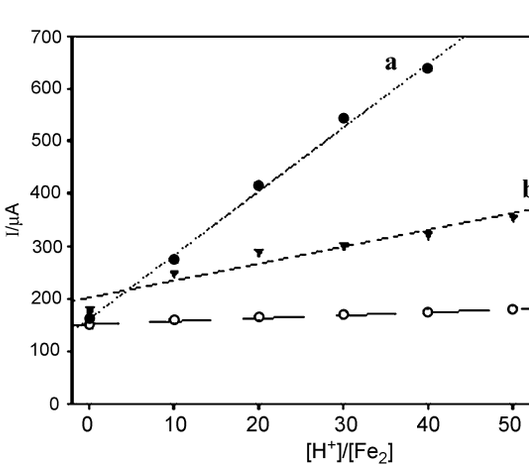

Fig. 6 Dependence of current heights of electrocatalytic waves on acid concentration. (a) **1-P** (−1.91 V), (b) **1** (−1.94 V) and (c) **1** (−1.31 V).

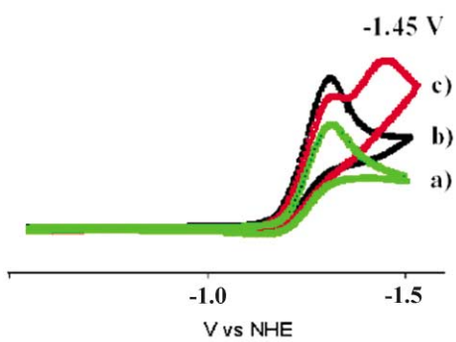

Fig. 7 Cyclic voltammograms of complex **1** (2.5 mM); (a) without acetic acid under N_2, (b) with acetic acid (50 mM) under CO and (c) with acetic acid (50 mM) under N_2.

Mechanisms

Our results point to two reductive routes to electrocatalysis of H_2 production from binuclear Fe^IFe^I complexes in the presence of weak acid, HOAc, as a proton source. For the all-CO complexes, the electrocatalysis occurs at the second reduction potential (E_2) that corresponds to an Fe^0Fe^0 species. The Fe^{II}–hydride that results from oxidative addition of a proton to Fe^0 is set up to accept another proton, generating an $(\eta^2\text{-}H_2)Fe^{II}–Fe^0$ complex according to Scheme 1. An EECC (electrochemical–electrochemical–chemical–chemical) mechanism accounts for this process.

With the PMe_3 substituents in the Fe^IFe^I complexes the Fe^0Fe^0 state is not accessible within the solvent window, however the electrocatalysis occurs at the Fe^0Fe^I oxidation level that is analogous to that expected for the $[Fe]H_2$ase enzyme active site.[17,18] Thus the $(\eta^2\text{-}H_2)Fe^{II}–Fe^I$ intermediate is a key species in

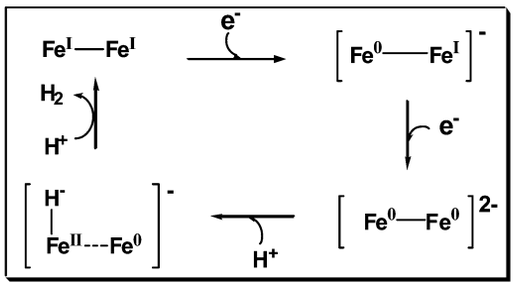

Scheme 1 Proposed EECC electrocatalysis mechanism for H_2 production of the all-CO complexes with H^+ invoking the second reduction potential.

several electrochemical pathways, deriving from Fe^I complexes as starting points. The ECCE (electrochemical–chemical–chemical–electrochemical) process as shown in Scheme 2(a) applies to the Fe^I–Fe^I model complexes, (μ-SRS)[$Fe(CO)_2L]_2$ (L = CO (*ca.* −1.2 to −1.3 V) and PMe_3 (−1.8 to −1.9 V)), with HOAc in CH_3CN. An alternative EC (electrochemical–chemical) route expressed in Scheme 2(b) can be proposed based on the bimolecular reaction of two Fe^{II}–hydride (H–Fe^{II}–Fe^I) species derived from oxidative addition of two protons to two separate Fe^0Fe^I species. Such an EC mechanism was previously proposed to account for the electrocatalysis of H_2 production by the mononuclear complex, $(\eta^5\text{-}C_5H_5)Co(PR_3)_2$.[31] Whether the formation of a tetranuclear cluster intermediate from two [H–$Fe^{II}Fe^I$] species is reasonable is not clear; it is poorly favored by steric factors.

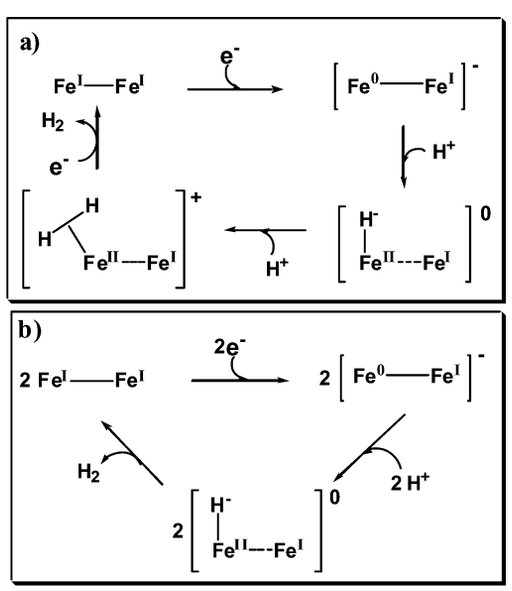

Scheme 2 Possible electrocatalysis mechanisms for H_2 production from Fe^IFe^I, (μ-SRS)[$Fe(CO)_2(PMe_3)]_2$ complexes and H^+: (a) ECCE and (b) EC.

Concluding remarks

Our studies have focused on a low-valent/weak acid route to H_2 production *via* electrocatalysis by dinuclear iron compounds, (μ-SRS)[$Fe^I(CO)_2L]_2$ (L = CO, PMe_3). In related studies, a neutral and an anionic mixed ligand complexes, (μ-pdt)[$Fe(CO)_2$-(PMe_3)][$Fe(CO)_2(L')]^z$ (L′ = PMe_3, z = 0; L′ = CN^-, z = −1) were reported by Rauchfuss and co-workers[28,29] to serve as electrocatalysts for H_2 production in the presence of strong acids, HOTs (toluenesulfonic acid), H_2SO_4 and HCl. The proposed catalytic mechanism in both cases is initiated by protonation of the Fe–Fe bond, followed by reduction of the resulting Fe^{II}(μ-H)Fe^{II} species to produce a Fe^I(μ-H)Fe^{II} intermediate and finally release H_2.[28,29] As the Rauchfuss system accesses the electrocatalysis with strong acids, it is reasonable that the electrochemical cycle has an alternate starting point.

With the weak CH_3COOH acid proton source as in our studies, even the bis-phosphine derivatives of the neutral complexes do not take up a proton in binuclear oxidative addition. Reduction at substantially negative potentials is required whereupon protonation immediately results in H_2 evolution; the well-known stable bridging hydride complex was never observed. This suggests single site oxidative addition of a proton to Fe^0 to give Fe^{II}–H, and after the second H^+ addition, (η^2-H_2)–Fe^{II}. The redox level at which the electrocatalysis takes place (Fe^0Fe^0 or Fe^0Fe^I) depends on the donor ability of the ligands. In the case of the PMe_3 derivatives, electrocatalytic H_2 production is observed from the Fe^0Fe^I redox state while the all-CO complexes show better electrocatalytic activity at the Fe^0Fe^0 than at the Fe^0Fe^I redox level. The better electrocatalytic activity of the PMe_3-derivatives at the Fe^IFe^0 level relative to the all-CO complexes is explained by the role of the good donor ligands in stabilizing the resulting H–Fe^{II} intermediate that is formed after the oxidative addition of a H^+ to Fe^0. It also provides a rationale for the necessity of the CN^- ligands at the active site of [Fe]H_2ase in terms of access to reversibility in H_2 uptake/production.

While the H_2 production activities of [Fe]H_2ase model complexes are much lower than that of the enzyme, they have offered opportunity to explore electrocatalysis mechanisms (ECCE, EC and EECC) and useful information for understanding the reactivity of each redox level (Fe^IFe^I, Fe^0Fe^I and Fe^0Fe^0) of hydrogenase model complexes for H^+ reduction. Interestingly, the recognition that binuclear complexes might be suitable functional models of hydrogenases has been an aspect of H_2-production electrocatalyst design long before the structures of [NiFe]- and [Fe]-H_2ase were established.[33] Even with the blueprint for H_2ase active site construction given by protein crystal structures, the critical features that allow the mild redox potentials of the biological catalyst have not been achieved in a synthetic system. In our study described above, a +300 mV gain in the reduction potential of acetic acid in non-aqueous solvent was achieved. Nevertheless the diiron complexes studied here have many points of modification, including the attachment of water-solubilizing pendant groups, studies of which are underway.

The simplicity of the [Fe]H_2ase active site as compared to that of [NiFe]H_2ase has, through model complexes, led to a better understanding of mechanisms of the redox levels that control H_2 production and H_2 uptake in the former.[35] It should be mentioned that although an iron–diatomic ligand moiety, (μ-$SR)_2Fe(CN)_2(CO)$, exists in the [NiFe]H_2ase active site, H_2 uptake is presumed to occur at nickel. Indeed, electrocatalytic H_2 generation has been observed with nickel-based biomimetic complexes as electrocatalyst.[36,37]

Acknowledgements

We acknowledge financial support from the National Science Foundation (Grants CHE-01-11629 to M. Y. D. for this work and CHE-0092010 for the EPR instrument) and contributions from the R. A. Welch Foundation to M. P. S. and M. Y. D. We thank our group members Dr Xuan Zhao and Chao-Yi Chiang for providing some of the compounds studied. R. M. R. gratefully acknowledges the Universidad Autonoma de Queretaro and PROMEP for their support. We thank Prof. W. Shin (Sogang University) for helpful discussions and an anonymous reviewer for suggestions.

References

1 P. M. Vignais, B. Billoud and J. Meyer, *FEMS Microbiol. Rev.*, 2001, **25**, 455–501.

2 R. Cammack, M. Frey and R. Robson, *Hydrogen as a Fuel: Learning from Nature*, Taylor & Francis, London and New York, 2001 and references therein.
3 M. W. W. Adams and E. I. Stiefel, *Science*, 1998, **282**, 1842–1843.
4 A. K. Jones, E. Sillery, S. P. J. Albracht and F. A. Armstrong, *Chem. Commun.*, 2002, 866–867.
5 S. V. Morozov, P. M. Vignais, L. Cournac, N. A. Zorin, E. E. Karyakina, A. A. Karyakin and S. Cosnier, *Int. J. Hydrogen Energy*, 2002, **27**, 1501–1505.
6 R. Cammack, *Nature*, 1999, **397**, 214–215.
7 J. W. Peters, W. N. Lanzilotta, B. J. Lemon and L. C. Seefeldt, *Science*, 1998, **282**, 1853–1858.
8 Y. Nicolet, C. Piras, P. Legrand, C. E. Hatchikian and J. C. Fontecilla-Camps, *Structure*, 1999, **7**, 13–23.
9 Y. Nicolet, A. L. De Lacey, X. Vernéde, V. M. Fernandez, E. C. Hatchikian and J. C. Fontecilla-Camps, *J. Am. Chem. Soc.*, 2001, **123**, 1596–1601.
10 A. Volbeda, M.-H. Charon, C. Piras, C. E. Hatchikian, M. Frey and J. C. Fontecilla-Camps, *Nature*, 1995, **373**, 580–586.
11 D. Seyferth, G. B. Womack, M. K. Gallagher, M. Cowie, B. Hames, J. P. Fackler, Jr. and A. M. Mazany, *Organometallics*, 1987, **6**, 283–294.
12 X. Zhao, I. P. Georgakaki, M. L. Miller, J. C. Yarbrough and M. Y. Darensbourg, *J. Am. Chem. Soc.*, 2001, **123**, 9710–9711.
13 X. Zhao, I. P. Georgakaki, M. L. Miller, R. Mejia-Rodriguez, C.-Y. Chiang and M. Y. Darensbourg, *Inorg. Chem.*, 2002, **41**, 3917–3928.
14 I. P. Georgakaki, M. L. Miller and M. Y. Darensbourg, *Inorg. Chem.*, 2003, **42**, 2489–2494.
15 G. J. Kubas, *Metal Dihydrogen and σ-Bond Complexes; Structure, Theory, and Reactivity*, Kluwer Academic/Plenum Press, New York, 2001.
16 C. V. Popescu and E. Münck, *J. Am. Chem. Soc.*, 1999, **121**, 7877–7884.
17 B. Bennet, B. J. Lemon and J. W. Peters, *Biochemistry*, 2000, **39**, 7455–7460.
18 A. L. De Lacey, C. Stadler, C. Cavazza, E. C. Hatchikian and V. M. Fernandez, *J. Am. Chem. Soc.*, 2000, **122**, 11232–11233.
19 E. J. Lyon, I. P. Georgakaki, J. H. Reibenspies and M. Y. Darensbourg, *J. Am. Chem. Soc.*, 2001, **123**, 3268–3278.
20 S. F. A. Kettle and L. E. Orgel, *J. Chem. Soc.*, 1960, 3890–3895.
21 L. F. Dahl and C-H. Wei, *Inorg. Chem.*, 1963, **2**, 328–333.
22 M. Razavet, S. C. Davies, D. L. Hughes, J. E. Barclay, D. J. Evans, S. A. Fairhurst, X. Liu and C. J. Pickett, *Dalton Trans.*, 2003, 586–595.
23 A. J. Bard, *Electrochemical Methods: Fundamentals and Applications*, Wiley, New York, 2001.
24 W-F. Liaw, C. Kim, M. Y. Darensbourg and A. L. Rheingold, *J. Am. Chem. Soc.*, 1989, **111**, 3591–3597.
25 CO solutions were quantitated by the infrared band of free CO at 2128 cm^{-1} by using CO-saturated CH_3CN as a standard.
26 E. J. Lyon, Ph. D. Dissertation, December 2000, Texas A&M University.
27 K. Izutsu, *Acid–Base Dissociation Constants in Dipolar Aprotic Solvents*; Blackwell Scientific Publications, Oxford, 1990, vol. 35.
28 F. Gloaguen, J. D. Lawrence and T. B. Rauchfuss, *J. Am. Chem. Soc.*, 2001, **123**, 9476–9477.
29 F. Gloaguen, J. D. Lawrence, T. B. Rauchfuss, M. Bénard and M-M. Rohmer, *Inorg. Chem.*, 2002, **41**, 6573–6582.
30 D. Astruc, *Electron Transfer and Radical Process in Transition-Metal Chemistry*, VCH, New York, 1995.
31 U. Koelle and S. Ohst, *Inorg. Chem.*, 1986, **25**, 2689–2694.
32 I. Bhugun, D. Lexa and J.-M. Savéant, *J. Am. Chem. Soc.*, 1996, **118**, 3982–3983.
33 J. P. Collman, Y. Ha, P. S. Wagenknecht, M.-A. Lopez and R. Guilard, *J. Am. Chem. Soc.*, 1993, **115**, 9080–9088.
34 X. Zhao, C.-Y. Chiang, M. L. Miller, M. V. Rampersad and M. Y. Darensbourg, *J. Am. Chem. Soc.*, 2003, **125**, 518–524.
35 M. Y. Darensbourg, E. J. Lyon, X. Zhao and I. P. Georgakaki, *Proc. Natl. Acad. Sci.*, 2003, **100**, 3683–3688.
36 L. L. Efros, H. H. Thorp, G. W. Brudvig and R. H. Crabtree, *Inorg. Chem.*, 1992, **31**, 1722–1724.
37 G. Musie, J. H. Reibenspies and M. Y. Darensbourg, *Inorg. Chem.*, 1998, **37**, 302–310.